The Matched Window Reassignment

Maria Sandsten
Mathematical Statistics,
Centre for Mathematical Sciences,
Lund University, Sweden
Email: sandsten@maths.lth.se

Johan Brynolfsson
Mathematical Statistics,
Centre for Mathematical Sciences,
Lund University, Sweden
Email: johanb@maths.lth.se

Isabella Reinhold
Mathematical Statistics,
Centre for Mathematical Sciences,
Lund University, Sweden
Email: isabella@maths.lth.se

***Abstract*—In this paper we calculate reassigned spectrograms using the envelope of an arbitrary signal as matched window. We show that the matched window then give the perfectly localized reassignment for any time-translated and frequency-modulated transient signal with corresponding envelope. The general expressions of the corresponding scaled reassignment vectors are derived and the matched window reassignment is evaluated for time-frequency localization as well as for classification. The results show that the accuracy in time- and frequency location is high also when the signal envelope deviates from the matched window and when the SNR is reasonable large. The classification performance based on the matched window reassignment and the Rényi entropy is robust to signal envelope deviations as well as to disturbing noise.**

I. Introduction

The reassignment technique, with the aim to improve the localization of a single time-frequency (TF) component and to enhance the readability of the TF representation, is introduced by [1]–[3]. The method reassigns signal energy to the center of gravity, giving higher energy concentration at the instantaneous frequencies of the signal. A similar method, the synchrosqueezing transform by [4], related to the empirical mode decomposition [5], reassigns all energy in frequency at a certain time point. However these methods only work well for longer chirps and constant frequency signals. Methods exist that convert the possible non-linear instantaneous frequency into a linear one and in [6] a nonlinear squeezing transform, especially designed for weak signal detection, is proposed.

Short transient signals are often modeled with a Gaussian envelope in time and TF based methods, such as Gabor and wavelet based algorithms have been applied to a large extent, for which the main aim is to find the analysis window achieving the best TF resolution, [7], [8]. We have proposed a method, where the reassignment procedure is rescaled to achieve the perfectly localized spectrogram of a Gaussian enveloped oscillating transient [9]. Using the Gaussian function window the TF concentration is superior to the usual reassignment, which in this specific case has been shown to give a circle or an ellipse as a result [10]. The optimal concentration increases the resolution performance beyond the lower bound of the Gabor transform [11]. With use of this technique we also estimate the parameters detailing oscillating Gaussian functions in a two-step procedure [11], [12]. Additionally, we have shown that the second Hermite function similarly can be used as matched window with resulting perfect localization, [13]. In this paper we show that perfect localization can be achieved for any signal, using the scaled reassignment and a matched window function.

In Section 2, the reassigned spectrogram is presented and in Section 3 the novel case of matched window reassignment is derived. Section 4 presents some simulations, especially for disturbing noise and jittering in the parameters of the matching windows. Section 5 concludes the paper.

II. Reassigned spectrogram

The short-time Fourier transform (STFT) of the signal $x(t)$ using the window $h(t)$ where integrals run from $-\infty$ to ∞ is

$$F_x^h(t,\omega) = \int x(s)h^*(s-t)e^{-i\omega s}ds, \tag{1}$$

and the corresponding spectrogram is found as

$$S_x^h(t,\omega) = |F_x^h(t,\omega)|^2. \tag{2}$$

The reassigned spectrogram, where the spectrogram values are relocated to the corresponding $\hat{t}_x$ and $\hat{\omega}_x$, is defined as

$$RS_x^h(t,\omega) = \iint S_x^h(s,\xi)\delta(t-\hat{t}_x(s,\xi),\omega-\hat{\omega}_x(s,\xi))dsd\xi, \tag{3}$$

where the two-dimensional Dirac impulse is defined as

$$\iint f(t,\omega)\delta(t-t_0,\omega-\omega_0)dtd\omega = f(t_0,\omega_0). \tag{4}$$

Introducing the scaling factors c_t and c_ω, the reassignment can be computed as

$$\hat{t}_x(t,\omega) = t + c_t\Re\left(\frac{F_x^{th}(t,\omega)}{F_x^h(t,\omega)}\right), \tag{5}$$

$$\hat{\omega}_x(t,\omega) = \omega - c_\omega\Im\left(\frac{F_x^{dh/dt}(t,\omega)}{F_x^h(t,\omega)}\right), \tag{6}$$

where $F_x^{th}(t,\omega)$ and $F_x^{dh/dt}(t,\omega)$ are STFTs of the signal $x(t)$, where $t\cdot h(t)$ and $dh(t)/dt$ are used as window functions, respectively. Further, $\Re(\bullet)$ and $\Im(\bullet)$ represents the real and imaginary parts respectively. If c_t and c_ω equals one the relocation is identical to the usual reassignment, [2].

ISBN 978-90-827970-1-5

III. Matched window reassignment

A transient oscillating signal is defined as

$$y(t) = a(t-t_0)e^{i\omega_0 t+\phi}, \tag{7}$$

where $a(t)$ represents the envelope of the oscillation and ϕ is the phase. As the quadratic class of distributions obey TF shift-invariance, all further analysis can be restricted to $x(t) = a(t)$, with time- and frequency center $t_0 = \omega_0 = 0$. We assume that the window $h(t) = x(-t)$. To find the reassignment vectors the functions to be derived are accordingly $F_x^h(t,\omega)$, $F_x^{th}(t,\omega)$ and $F_x^{dh/dt}(t,\omega)$ in Eqs. (5,6). The STFT in Eq. (1) is accordingly defined as

$$F_x^h(t,\omega) = \int x(s)x(t-s)e^{-i\omega s}ds. \tag{8}$$

With $s = s_1 + t/2$ we get

$$\begin{aligned} F_x^h(t,\omega) &= e^{-i\frac{\omega t}{2}}\int x(s_1+\frac{t}{2})x(\frac{t}{2}-s_1)e^{-i\omega s_1}ds_1 \\ &= e^{-i\frac{\omega t}{2}}R_1(t,\omega), \end{aligned} \tag{9}$$

where

$$R_1(t,\omega) = \int x(s_1+\frac{t}{2})x(\frac{t}{2}-s_1)e^{-i\omega s_1}ds_1, \tag{10}$$

is real-valued as the expression $x(s_1+\frac{t}{2})x(\frac{t}{2}-s_1)$ is an even function around $s_1 = 0$ for all values of t. We also find

$$F_x^{th}(t,\omega) = \int x(s)(s-t)x(t-s)e^{-i\omega s}ds, \tag{11}$$

where $th(t) = tx(-t)$. Expanding the integral in Eq. (11) as

$$F_x^{th}(t,\omega) = \int x(s)(s-\frac{t}{2})x(t-s)e^{-i\omega s}ds - \frac{t}{2}F_x^h(t,\omega), \tag{12}$$

and further use the same replacement of variables as in Eq. (9) we find

$$\begin{aligned} F_x^{th}(t,\omega) &= e^{-i\frac{\omega t}{2}}\int s_1 x(s_1+\frac{t}{2})x(\frac{t}{2}-s_1)e^{-i\omega s_1}ds_1 - \\ &\quad e^{-i\frac{\omega t}{2}}\frac{t}{2}R_1(t,\omega) \\ &= e^{-i\frac{\omega t}{2}}(I_1(t,\omega) - \frac{t}{2}R_1(t,\omega)), \end{aligned} \tag{13}$$

where the function $I_1(t,\omega)$ will be purely imaginary as $s_1 x(s_1+\frac{t}{2})x(\frac{t}{2}-s_1)$ is always an odd function around $s_1 = 0$ independently of t. Accordingly the real part of the ratio in Eq. (5) is

$$\Re\left(\frac{F_x^{th}(t,\omega)}{F_x^h(t,\omega)}\right) = \Re\left(\frac{e^{-i\frac{\omega t}{2}}(I_1(t,\omega)-\frac{t}{2}R_1(t,\omega))}{e^{-i\frac{\omega t}{2}}R_1(t,\omega)}\right),$$

where $e^{-i\frac{\omega t}{2}}$ are canceled in the denominator and numerator. As $I_1(t,\omega)$ is purely imaginary, the real part will simplify to

$$\Re\left(\frac{F_x^{th}(t,\omega)}{F_x^h(t,\omega)}\right) = -\frac{t}{2}. \tag{14}$$

For the STFT using the derivative of the window we have

$$\frac{dh(t)}{dt} = -x'(-t), \tag{15}$$

rendering

$$\begin{aligned} F_x^{\frac{dh}{dt}}(t,\omega) &= -\int x(s)x'(t-s)e^{-i\omega s}ds \\ &= -\frac{1}{2\pi}\int i\nu X(\nu)X(\nu+\omega)e^{i\nu t}d\nu, \end{aligned} \tag{16}$$

where $X(\nu)$ is the Fourier transform $X(\nu) = \int x(t)e^{-i\nu t}dt$. With $\nu = \nu_1 - \omega/2$ the integral in Eq. (16) is expanded as

$$= \frac{e^{-i\frac{\omega t}{2}}}{2\pi}\int i(\frac{\omega}{2}-\nu_1)X(\nu_1-\frac{\omega}{2})X(\nu_1+\frac{\omega}{2})e^{i\nu_1 t}d\nu_1. \tag{17}$$

We focus on

$$X(\nu_1-\frac{\omega}{2})X(\nu_1+\frac{\omega}{2}) = C_x^{\Re}(\nu_1,\omega) + iC_x^{\Im}(\nu_1,\omega), \tag{18}$$

where $C_x^{\Re}(\nu_1,\omega)$ is an even function around $\nu_1 = 0$ independently of ω and similarly $C_x^{\Im}(\nu_1,\omega)$ is always an odd function. Then the integral

$$I_2(t,\omega) = \frac{1}{2\pi}\int \nu_1 X(\nu_1-\frac{\omega}{2})X(\nu_1+\frac{\omega}{2})e^{i\nu_1 t}d\nu_1, \tag{19}$$

will be purely imaginary. The integral

$$R_2(t,\omega) = \frac{1}{2\pi}\int X(\nu_1-\frac{\omega}{2})X(\nu_1+\frac{\omega}{2})e^{i\nu_1 t}d\nu_1, \tag{20}$$

will not only be purely real-valued but also it will hold that $R_2(t,\omega) = R_1(t,\omega)$, as

$$\begin{aligned} &R_2(t,\omega) \\ &= \frac{1}{2\pi}\int X(\nu_1-\frac{\omega}{2})X(\nu_1+\frac{\omega}{2})e^{i\nu_1 t}d\nu_1 \\ &= \frac{1}{2\pi}\int X(\nu_1-\frac{\omega}{2})\left[\int x(s)e^{-i\frac{\omega}{2}s}e^{-i\nu_1 s}ds\right]e^{i\nu_1 t}d\nu_1 \\ &= \frac{1}{2\pi}\int\left[\int X(\nu_1-\frac{\omega}{2})e^{i\nu_1 t}e^{-i\nu_1 s}d\nu_1\right]x(s)e^{-i\frac{\omega}{2}s}ds \\ &= \frac{1}{2\pi}\int 2\pi x(-s+t)x(s)e^{-i\omega(s-\frac{t}{2})}ds. \end{aligned} \tag{21}$$

With $s_1 = s - t/2$ we get

$$R_2(t,\omega) = \int x(\frac{t}{2}-s_1)x(s_1+\frac{t}{2})e^{-i\omega s_1}ds_1 = R_1(t,\omega). \tag{22}$$

Hence, we have

$$F_x^{\frac{dh}{dt}}(t,\omega) = e^{-i\frac{\omega t}{2}}\left(i\frac{\omega}{2}R_1(t,\omega) - iI_2(t,\omega)\right). \tag{23}$$

and

$$\Im\left(\frac{F_x^{\frac{dh}{dt}}(t,\omega)}{F_x^h(t,\omega)}\right) = \Im\left(\frac{e^{-i\frac{\omega t}{2}}\left(i\frac{\omega}{2}R_1(t,\omega) - iI_2(t,\omega)\right)}{e^{-i\frac{\omega t}{2}}R_1(t,\omega)}\right).$$

The imaginary part of Eq. (6) will simplify to

$$\Im\left(\frac{F_x^{\frac{dh}{dt}}(t,\omega)}{F_x^h(t,\omega)}\right) = \frac{\omega}{2}. \tag{24}$$

With this approach the reassignment vectors simplify to

$$\hat{t}_x(t,\omega) = t - c_t\frac{t}{2}, \tag{25}$$

$$\hat{\omega}_x(t,\omega) = \omega - c_\omega\frac{\omega}{2}, \tag{26}$$

ISBN 978-90-827970-1-5 © EURASIP 2018

and with the scaled reassignment $c_t = c_\omega = 2$ as proposed in [9] for the matched Gaussian window, and in [13] for the matched second Hermite function, all signal energy are reassigned to $\hat{t}_x(t,\omega) = \hat{\omega}_x(t,\omega) = 0$. Accordingly, due to the TF shift invariance, the envelope matched window $h(t) = a(-t)$ gives the perfect localized reassignment at $\hat{t}_x(t,\omega) = t_0$ and $\hat{\omega}_x(t,\omega) = \omega_0$ for all possible $y(t)$ in Eq. (7).

IV. Simulation examples

We illustrate with an example signal, simulated from the envelope of

$$a_0(t) = \sum_{k=1}^{K} \alpha_k q_k(t), \tag{27}$$

where $q_k(t)$, $k = 1 \dots K$ are a set of basis Hermite functions and α_k some chosen weights. The example envelope is given from $K = 4$ Hermite functions and α_k given as 1, -0.5, 0 and 0.5 for $k = 1 \dots 4$, with the resulting envelope illustrated in Figure 1a). A three-component signal with components given from Eq. (7), all with equal amplitudes and envelope shapes but different time locations, t_0, as 70, 140 and 200 and and oscillating frequencies, ω_0 $2\pi 0.125$, $2\pi 0.3$ and $2\pi 0.2$, is illustrated in Figure 1b). All phases ϕ are $U[-\pi, \pi]$. The corresponding usual matched spectrogram (MSP), where naturally $h(t) = a_0(t)$, and the matched window reassignment (MWR), i.e., $h(t) = a_0(-t)$ are presented in Figure 2a) and b) respectively. It is easily verified that the peaks found in Figure 2b) are the exact time locations and the exact value (or closest discrete Fourier transform-bin) for the frequency locations. We should point out that it is no limitation to consider only the one-component case in the following simulations as the reassignment is a TF local operation, independent of time- and frequency location, as long as the components are reasonably separated. Additionally, the envelope shape used here, simulated from a sum of Hermite functions is just a model example and there is no limitations to use any other envelope shape.

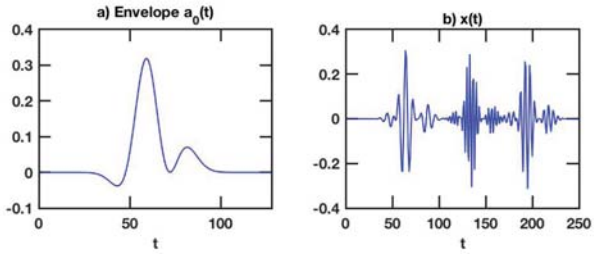

Fig. 1. a) An example envelope used as function basis; b) A three component example signal with the same envelope basis but where all components are individually shifted in time and frequency.

Many of the existing concentration measures in TF analysis are based on information or sparsity optimization where one of the most famous is the Rényi entropy (RE), [14], defined as

$$\mathrm{RE} = \frac{1}{1-\alpha} \log_2 \int\int \left(\frac{W_x(t,\omega)}{\int\int W_x(t,\omega) dt d\omega} \right)^{\alpha} dt d\omega, \tag{28}$$

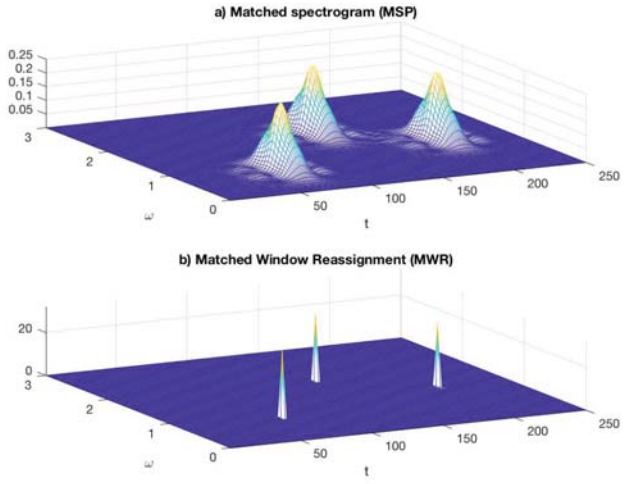

Fig. 2. a) The matched spectrogram (MSP) of the signal shown in Figure, 1b), containing three components with the same envelope. b) The corresponding matched window reassignment (MWR).

where $W_x(t,\omega)$ is any TF representation, and all integrals are assumed to run over a chosen region of the TF plane. The choice of the parameter $\alpha = 3$ is the most applied formulation [15] and for this choice the local RE for the peak of each component in Figure 2b) will be zero, the smallest possible entropy, where only one value differs from zero. For the three-components altogether, the RE becomes $1.66 \approx \log_2(3)$. Theoretically, the RE could be used for counting of the equal amplitude and equal envelope components, as the RE measure is simplified to $\log_2$(number of components).

A. Time-frequency localization performance

We simulate one-component signals with $t_0 = 64$ and $\omega_0 = 0.125$ using the envelope in Eq. (27) where we allow for a stochastic jitter in the parameters α_k according to

$$a(t) = \sum_{k=1}^{K} (\alpha_k + \sigma_p \Delta\alpha) q_k(t), \tag{29}$$

where $\Delta\alpha \in U[-1, 1]$ and σ_p is a parameter. We simulate 1000 realizations and the resulting envelopes are illustrated in Figure 3a) for $\sigma_p = 0.3$. The simulation is extended with additive zero mean Gaussian white noise, for different signal-to-noise ratios (SNR), where SNR is defined as the average power of the signals divided by the variance of the noise.

We then apply the matched window reassignment (MWR) where $h(t) = a_0(-t)$. The maximum value of the TF representation is found and the estimate of $\hat{t}_0$ and $\hat{\omega}_0$ is taken as the corresponding time- and frequency location. The percentage of the number of correct time locations, i.e., $\hat{t}_0 - t_0 = 0$ is evaluated and depicted in Figure 4a) for different values of σ_p and different SNR. The degradation in accuracy for larger values of σ_p is caused by that the single peak is widened and at some occasions the nearby time value is the maximum peak. For SNR=10 dB it is obvious that the

ISBN 978-90-827970-1-5 © EURASIP 2018

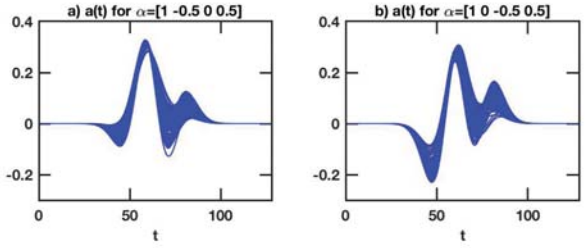

Fig. 3. The figures each show 1000 realizations of envelopes of two similar constructed classes. Each realization is given a random jittering of the parameters as presented in Eq. (29) for $\sigma_p = 0.3$. Note that the main visible difference is the depth of the first trough.

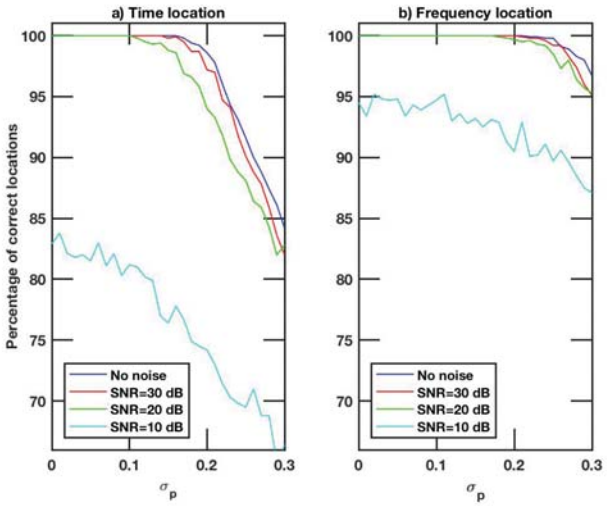

Fig. 4. The figures show the accuracy of the estimated time and frequency peak locations of the matched window reassignment. The evaluation is made on 1000 realizations with envelopes presented in Figure 3a) for different σ_p and four different levels of SNR; a) Percentage of correct time locations; b) Percentage of correct frequency locations.

results becomes inaccurate also when $\sigma_p = 0$, i.e., when the matched window is the exact shape of the envelope. In Figure 4b) the corresponding percentage of correct frequency locations $\hat{\omega}_0 - \omega_0 = 0$ is shown for the same range of σ_p and SNR. The results are similar to the estimated time locations although somewhat more accurate for larger σ_p and lower SNR. Studying the errors more closely we find that the nearby frequency bin is the maximum value in all deviant cases.

We also investigate the corresponding RE measures of this simulation shown in Figure 5a) that the mean RE of the 1000 simulations is robust to the increase in the jitter parameter σ_p when there is no additive noise. The mean $\pm$ one standard deviation are also depicted to show the variations of the measure. In Figure 5b) the mean RE is shown for the different cases of additive GWN and a large increase of RE is mainly seen for when SNR=10 dB, which also is the case where the time and frequency locations become more difficult to estimate with accuracy.

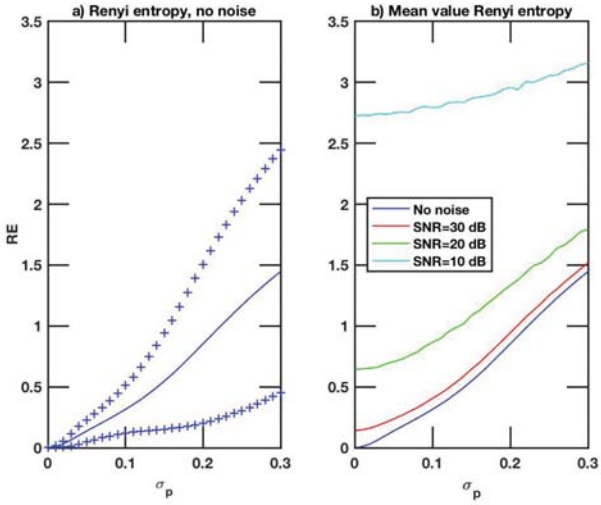

Fig. 5. a) The mean Rényi entropy as function of jitter parameter σ_p with $\pm$ one standard deviation shown as plus signs for the case of no noise; b) The mean Rényi entropies as functions of the jitter parameter σ_p for four different levels of SNR.

B. Classification performance

We also investigate the performance of classification when the window $h(t) = a_0(-t)$ as presented in Figure 3a) is used in MWR. We also compare with the MSP. Two classes should be differed, class I consisting of 1000 simulations according to the previous description for the envelope jitter and SNR. Class II is similar but the envelope is given according to Figure 3b). As seen, the two classes are close to overlap in envelope shape when σ_p is large. We also allow for a Gaussian distributed deviation in the time locations of $N(0, 10)$ and in the frequency locations of $N(0, 0.01)$. We will use the RE as classification measure but additionally we investigate the statistical kurtosis (SK), defined as

$$\text{SK} = \frac{\int\int W_x(t,\omega)^4 dt d\omega}{(\int\int W_x(t,\omega)^2 dt d\omega)^2}. \tag{30}$$

The SK measures the sharpness of a distribution and has been suggested in [16] as a TF concentration measure.

The resulting Receiver Operating Characteristics (ROCs) are shown in Figure 6a) and 7a) for two different SNR, and two different σ_p. The MWR outperforms the MSP and we can also see that using the RE measure is more reliable than using the SK measure in the evaluation. In Figure 6b) and 7b) the True Positive Rates (TPRs) are depicted for a range of the parameter σ_p when the False Positive Rate (FPR) is allowed to be 5%. The MWR using the RE as measure is shown to give a reliable classification also for low SNR.

We also evaluated using a simple correlation measure in time, where the matched window (filter) was correlated with the absolute values of the time signals, similarly to matched filter detection. The classification results were close to random in all cases and are not included in the figures. The main reason for the failure is the frequency jitter which effects a time based correlation significantly. This will also be the case

ISBN 978-90-827970-1-5 © EURASIP 2018

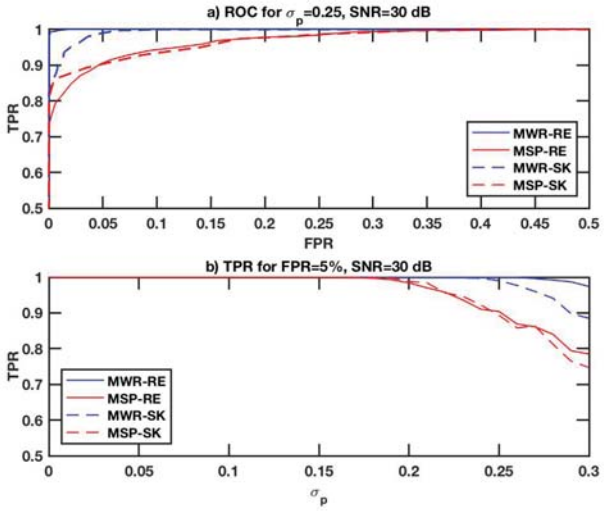

Fig. 6. a) The resulting ROC for $\sigma_p = 0.25$ and SNR=30 dB for the MWR and MSP, evaluated using the Rényi entropy (RE) and statistical kurtosis (SK) measures; b) The True Positive Rates (TPRs) as a function of the parameter σ_p when the False Positive Rate (FPR) is allowed to be 5% for SNR=30 dB.

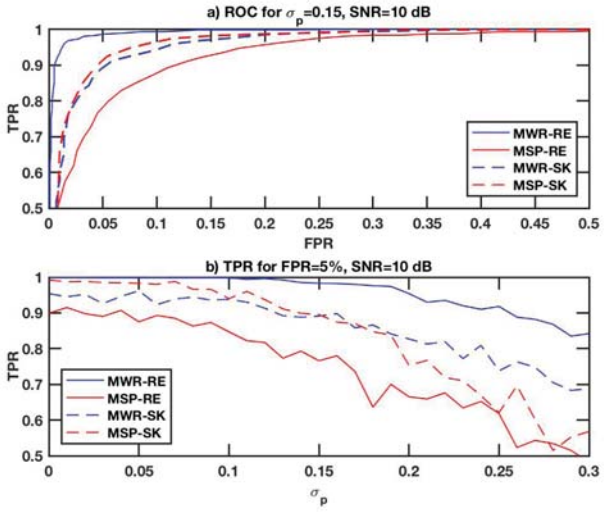

Fig. 7. a) The resulting ROC for $\sigma_p = 0.15$ and SNR=10 dB for the MWR and MSP, evaluated using the Rényi entropy (RE) and statistical kurtosis (SK) measures; b) The True Positive Rates (TPRs) as a function of the parameter σ_p when the False Positive Rate (FPR) is allowed to be 5% for SNR=10 dB.

for many other features and classification methods. However, for the MWR and MSP evaluated with the TF concentration measures, deviations in time- and frequency locations do not matter for the classification result.

V. Conclusions

A novel technique of matched window reassignment of the spectrogram is proposed with the aim to localize and classify transient functions of arbitrary shape. We derive the reassignment vectors that give perfect localization when the window match the envelope of the transient function. The method is evaluated for time- and frequency localization where the location of the maximum peak is the estimate. The results show that the accuracy in time- and frequency localization is high also when the signal envelope deviates from the matched window and when the SNR is reasonable large. In the classification example the Rényi entropy is shown to be a useful feature for distinction between classes. Other applications are easily found, e.g. when it is difficult to judge if a signal consists of a certain type of components, the method could be used as shape detector.

VI. Acknowledgments

The authors would like to thank the eSSENCE strategic research programme for funding.

References

[1] K. Kodera, C. de Villedary, and R. Gendrin, "A new method for the numerical analysis of nonstationary signals," *Physics of the Earth & Planetary Interiors*, vol. 12, pp. 142–150, 1976.

[2] F. Auger and P. Flandrin, "Improving the readability of time-frequency and time-scale representations by the reassignment method," *IEEE Transactions on Signal Processing*, vol. 43, pp. 1068–1089, May 1995.

[3] F. Auger, E. Chassande-Mottin, and P. Flandrin, "Making reassignment adjustable: The Levenberg-Marquardt approach," in *Proceedings of the ICASSP*. IEEE, 2012, pp. 3889–3892.

[4] I. Daubechies, J. Lu, and H.-T. Wu, "Synchrosqueezed wavelet transforms: An empirical mode decomposition-like tool.," *Applied & Computational Harmonic Analysis*, vol. 30, no. 2, pp. 243 – 261, 2011.

[5] N. E. Huang and Z. Wu, "A review on Hilbert-Huang transform: Method and its applications to geophysical studies.," *Reviews of Geophysics*, vol. 46, no. 2, 2008.

[6] S. Wang, X. Chen, Y. Wang, G. Cai, B. Ding, and X. Zhang, "Nonlinear squeezing time-frequency transform for weak signal detection.," *Signal Processing*, vol. 113, pp. 195 – 210, 2015.

[7] I. Reinhold, M. Sandsten, and J. Starkhammar, "Objective detection and time-frequency localization of components within transient signals," *Journal of the Acoustical Society of America (JASA)*, vol. 143, no. 4, 2018.

[8] S. Chandran, A. Mishra, V. Shirhatti, and R. Ray, "Comparison of matching pursuit algorithm with other signal processing techniques for computation of the time-frequency power spectrum of brain signals.," *The Journal Of Neuroscience*, vol. 36, no. 12, pp. 3399 – 3408, 2016.

[9] M. Hansson-Sandsten and J. Brynolfsson, "The scaled reassigned spectrogram with perfect localization for estimation of Gaussian functions," *IEEE Signal Processing Letters*, vol. 22, no. 1, pp. 100–104, 2015.

[10] P. Flandrin, "A note on reassigned Gabor spectrograms of Hermite functions," *J Fourier Analysis and Applications*, vol. 19, no. 2, pp. 285–295, 2013.

[11] J. Brynolfsson and M. Sandsten, "Parameter estimation of oscillating Gaussian functions using the scaled reassigned spectrogram," *Signal Processing*, vol. 150, pp. 20–32, 2018.

[12] J. Brynolfsson and M. Hansson-Sandsten, "Parameter estimation of Gaussian functions using the scaled reassigned spectrogram," in *EUSIPCO*, Nice, France, 2015.

[13] I. Reinhold, J. Starkhammar, and M. Sandsten, "The scaled reassigned spectrogram adapted for detection and localization of transient signals," in *EUSIPCO*, Kos island, Greece, 2017.

[14] W. J. Williams, M. L. Brown, and A. O. Hero, "Uncertainty, information, and time-frequency distributions," in *Proceedings SPIE Int. Soc. Opt. Eng.* SPIE, 1991, vol. 1566, pp. 144–156.

[15] R. G. Baraniuk, P. Flandrin, A. J. E. M. Janssen, and O. J. J. Michel, "Measuring time-frequency information content using Rényi entropies," *IEEE Transactions on Information Theory*, vol. 47, no. 4, pp. 1391–1409, May 2001.

[16] D. L. Jones and T. W. Parks, "A high-resolution data-adaptive time-frequency representation," *IEEE Transactions on Acoustics, Speech, and Signal Processing*, vol. 38, pp. 2127–2135, 1990.

ISBN 978-90-827970-1-5 © EURASIP 2018